# Kinetics of Single-Wall Carbon Nanotube Coating Displacement by Single-Stranded DNA Depends on Nanotube Structure

Kunhua Lei,† Sergei M. Bachilo,† and R. Bruce Weisman\*,†,‡

## **ABSTRACT**

Time-resolved fluorescence spectroscopy has been used to study the displacement of adsorbed sodium dodecyl sulfate (SDS) from the surface of single-wall carbon nanotubes (SWCNTs) by short strands of single-stranded DNA. Intensity changes in near-infrared emission peaks of various SWCNT structures were analyzed following the addition of six different  $(GT)_n$  oligomers (n from 3 to 20) to SDS-coated nanotube samples. There is a strong kinetic dependence on oligomer length, with (GT)<sub>3</sub> giving an initial rate more than 1000 times greater than that of (GT)<sub>20</sub>. For shorter oligos in the (GT)<sub>n</sub> series, we observe an inverse dependence of displacement rate on SWCNT diameter, with SDS displaced from (6,5) more than twice as fast as from (8,7). However, this diameter dependence is reversed for oligos with more than six (GT) units. There is also a systematic dependence of displacement rate on nanotube chiral angle that is strongest for (GT)5, leading to a factor of ~3 initial rate difference between (9,1) and (6,5) despite their identical diameters. To account for these findings, we propose a simple two-step kinetic model in which disruption of the original SDS coating is followed by conformational relaxation of the ssDNA on the nanotube surface. The relaxation is relatively fast for ssDNA oligos shorter than 12 base pairs, making the first step rate-determining. Conversely, relaxation of the longer oligos is slow enough that the second step becomes rate-determining.

Keywords: coating exchange kinetics; competitive adsorption; kinetic spectroscopy, nanotube enantiomers, SWCNT chiral angle effects, conformational relaxation

<sup>†</sup> Department of Chemistry and the Smalley-Curl Institute, Rice University, Houston, TX 77005 United States

<sup>&</sup>lt;sup>‡</sup> Department of Materials Science and NanoEngineering, Rice University, Houston, TX 77005 United States

Single-wall carbon nanotubes (SWCNTs) are well known for their unique electronic, <sup>1,2</sup> optical, <sup>3</sup> mechanical, <sup>4</sup> and chemical properties <sup>5</sup> that make them attractive subjects for fundamental studies and for a range of potential applications. One of the major challenges in utilizing carbon nanotubes is their tendency to aggregate and form bundles. To address this issue, a variety of surfactants and polymers have been used to non-covalently coat the surfaces of individualized nanotubes and stabilize them in aqueous suspensions. A very interesting family of nanotube coatings is short oligomers (oligos) of single-stranded DNA (ssDNA). These have been found to show selective affinities for different SWCNT structures that vary with the oligo nucleobase sequence. <sup>6</sup> Structure-selective interactions between SWCNTs and ssDNA are important for nanotube sorting, <sup>6–9</sup> biosensing, <sup>10–13</sup> and functionalization applications, <sup>14–16</sup> some of which involve the competitive adsorption of different coatings on nanotube surfaces.

Studies of coating exchange can provide practical guidance for nanotube processing and also improve basic understanding of nanotube-coating interactions. Prior research has focused on the displacement of ssDNA by conventional surfactants. Roxbury et al. 17 used absorption spectroscopy to monitor displacement of different ssDNA sequences from (6,5) SWCNTs by sodium dodecylbenzene sulfonate (SDBS). They deduced that the process is dominated by defects in the initial ssDNA coating. Subsequently, Shankar et al. used a similar method to study displacement by SDBS of three ssDNA oligos adsorbed on (6,5), (9,1), and (8,3) SWCNTs. <sup>18</sup> Large differences in measured activation energies were correlated with recognition behavior and attributed to SWCNT electronic properties. In 2017, Jena et al. applied fluorescence spectroscopy to track the displacement of six ssDNA oligos of different lengths ((GT)<sub>3</sub> to (GT)<sub>30</sub>) by the surfactant sodium deoxycholate (SDC) for six (n,m) species.<sup>19</sup> They found single-exponential kinetics that were not correlated with the spectral properties thought to reveal surface coverage by the ssDNA. A fluorescence-based 2018 study by Zheng et al. uncovered a 200-fold difference in the rates at which SDC displaces (ATT)<sub>4</sub> from the two enantiomers of (7.5) SWCNTs.<sup>20</sup> The time-resolved fluorescence approach was also used by Xhyliu and Ao in their 2020 report of a wide range of time constants for the displacement of various ssDNA oligos from (n,m)-purified SWCNT samples after addition of SDC. 21 Much less is known about the reverse exchange process, in which ssDNA displaces a conventional surfactant. The 2020 study by Yang et al. of SDC to ssDNA exchange involved addition of methanol to desorb the initial SDC, rather than a direct spontaneous displacement by added ssDNA.<sup>22</sup>

Here we report a kinetic study exploring direct SDS to ssDNA surfactant exchange. We have measured kinetics for 18 (n,m) species and six different ssDNA oligo lengths. The displacements were monitored with (n,m) selectivity using near-IR fluorescence spectroscopy, taking advantage of the sensitivity of SWCNT emission wavelengths and intensities to their surface environment. Our results reveal displacement kinetics that depend on ssDNA length, on nanotube diameter, on nanotube chiral (roll-up) angle, and possibly also on nanotube handedness.

#### RESULTS AND DISCUSSION

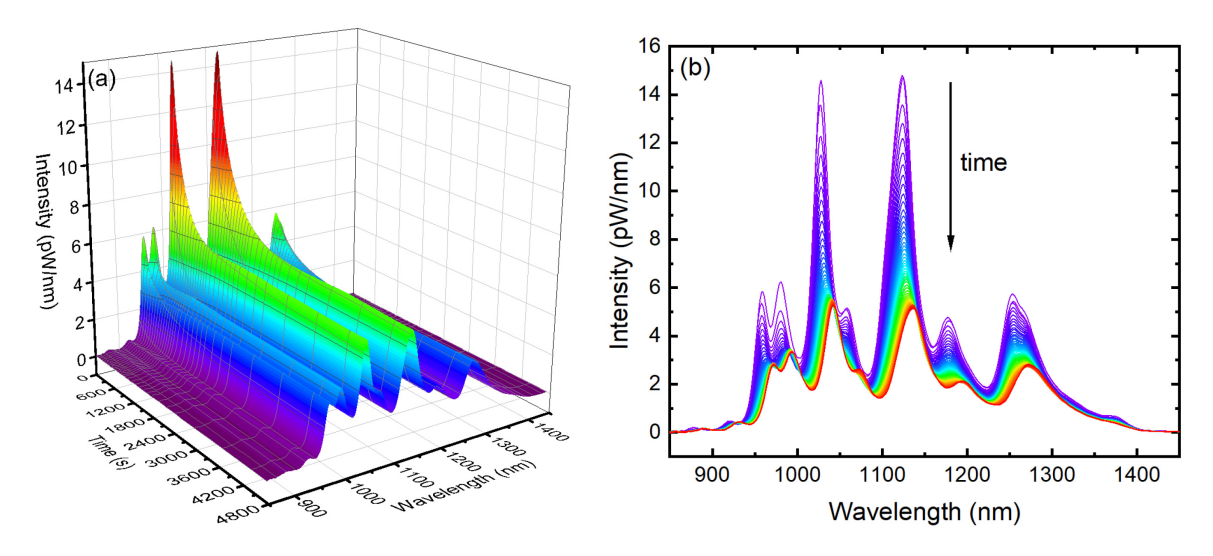
## **Experimental Approach**

Fluorescence spectroscopy is an incisive monitor of SWCNT coating displacement because the nanotube emission wavelengths and quantum yields are sensitive to local environment. Displacement of SDS by ssDNA red-shifts the SWCNT peaks and lowers their intensities. We explored the effect of ssDNA length through a series of displacement kinetics experiments using six  $(GT)_n$  oligos, with n equal to 3, 5, 6, 8, 12, and 20. Variations in displacement kinetics among SWCNT structures were extracted by analyzing different spectral peaks known to arise from specific (n,m) species.  $^{23-25}$  We note that coating displacement in these experiments was aided by using samples initially dispersed in an SDS solution with a concentration of only 0.15% (w/v), which is near or below the critical micelle concentration in pure water but sufficient to form stable nanotube suspensions.

#### **Kinetic Analysis using Initial Rates**

Factors complicating kinetic analysis of the data in this project include time-dependent spectral overlaps among peaks, unknown kinetic rate laws, and decreases in free ssDNA concentration as displacement proceeds. To reduce effects from spectral overlap, we used a set of five excitation wavelengths (580 nm, 640 nm, 674 nm, 727 nm, 790 nm) that provided near-resonant excitation of different sets of (n,m) species, thus intensifying their peaks relative to others. We addressed other complications by extracting initial rate constants without reference to a full kinetic model.

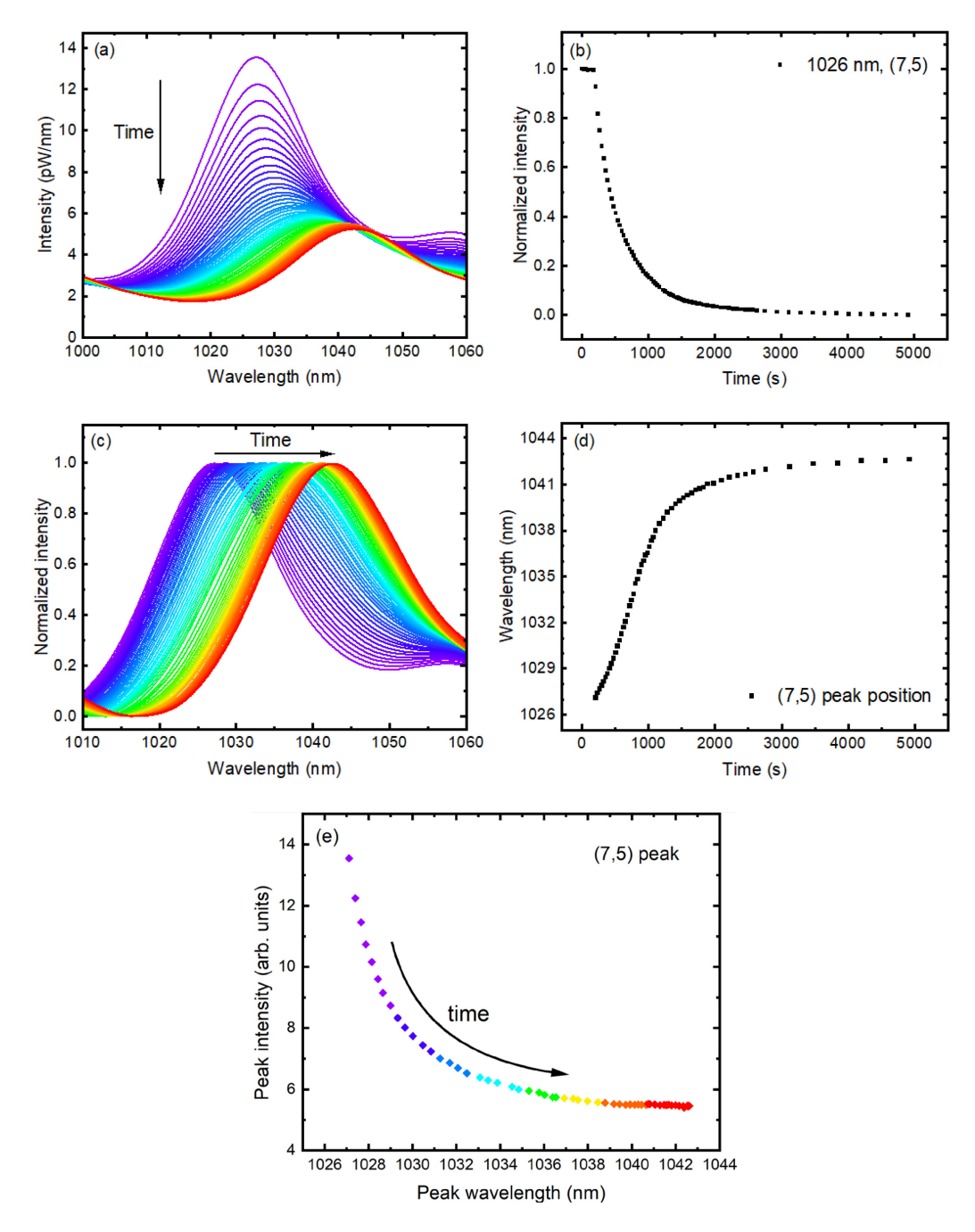
As an example of the observed data, we plot in Figure 1 the time-sequenced emission spectra measured using 640 nm fluorescence excitation while (GT)<sub>5</sub> displaced the SDS. (Spectra measured during the same run with the other four excitation wavelengths are shown in Figure S1.) As seen



**Figure 1.** Time-resolved emission spectra of SWCNTs coating displacement kinetics from SDS to ssDNA. The figure shows one of example data sets. Single-stranded DNA is (GT)<sub>5</sub>. The excitation wavelength is 640 nm. Emission intensity dropping with time is illustrated in the left-hand side (a) 3D graph. Color change from bright red to dark purple emphasizes fluorescence intensity decrease. The same data was plotted in 2D as right-hand side figure (b) to show the emission peak red-shift, which was illustrated by color change from purple to red.

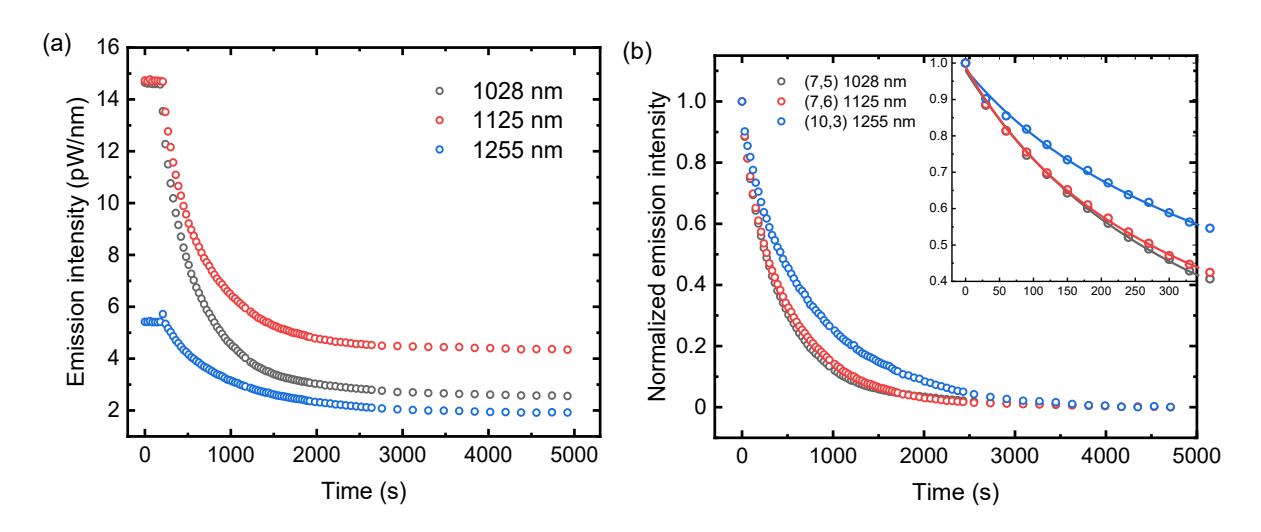
in Figure 1b, the SWCNT emission peaks decreased in intensity and shifted to longer wavelengths after the addition of ssDNA. The two prominent peaks in Figure 1b represent (7,5) and (7,6) SWCNTs (wavelength ranges 1026 - 1041 nm and 1123 - 1135 nm, respectively). Focusing on changes in the (7,5) emission region, we display the raw spectra in Figure 2a and normalized spectra in Figure 2c. Figure 2b shows the decreasing emission intensity at 1026 nm (the peak wavelength in 0.15% SDS) as a function of time after ssDNA addition, and Figure 2d shows the monotonic increase of peak wavelength during the same period. The correlation between peak intensity and peak wavelength of the (7,5) emission during this displacement process is plotted in Figure 2e. We extracted analogous spectral data for multiple (n,m) peaks using several excitation wavelengths and all six of the studied  $(GT)_n$  ssDNA oligos.

Figure 3a shows the time-dependent fluorescence intensities measured at the emission peaks of (7,5), (7,6), and (10,3) SWCNTs. The constant values before 210 s (the time of ssDNA injection) confirm stable emission until the start of displacement by the added (GT)<sub>5</sub>. To determine initial rate constants, we adjusted the time zero to match the injection time and re-scaled the intensity values between 0 and 1 by subtracting the long time asymptote and then dividing by the difference between the pre-injection intensity and that asymptote. This gave the normalized traces shown in



**Figure 2.** (a) Displacement kinetics of (7,5) species from SDS-coated to ssDNA-coated; (b) Emission intensity change vs. time at 1026 nm; (c) Normalized spectra from panel (a); (d) Peak position of (7,5) emission vs. time; (e) Correlation between peak intensity and peak wavelength during coating displacement.

Figure 3b. Regardless of the form of the full kinetic trace, one can characterize the initial decay by an apparent first-order rate constant evaluated as the initial slope divided by the initial magnitude



**Figure 3.** Initial rate analysis of fluorescence data excited at 640 nm. The plot analyzed different initial rates of (7,5), (7,6) and (10,3) species right after adding ssDNA (GT)<sub>5</sub>. The emission intensity of whole process was normalized. The insert figure is a zoom-in in the beginning phase. A fitting function is applied for the data points in the first few minutes. Taking the derivative at time equal to zero gives the initial rate constant.

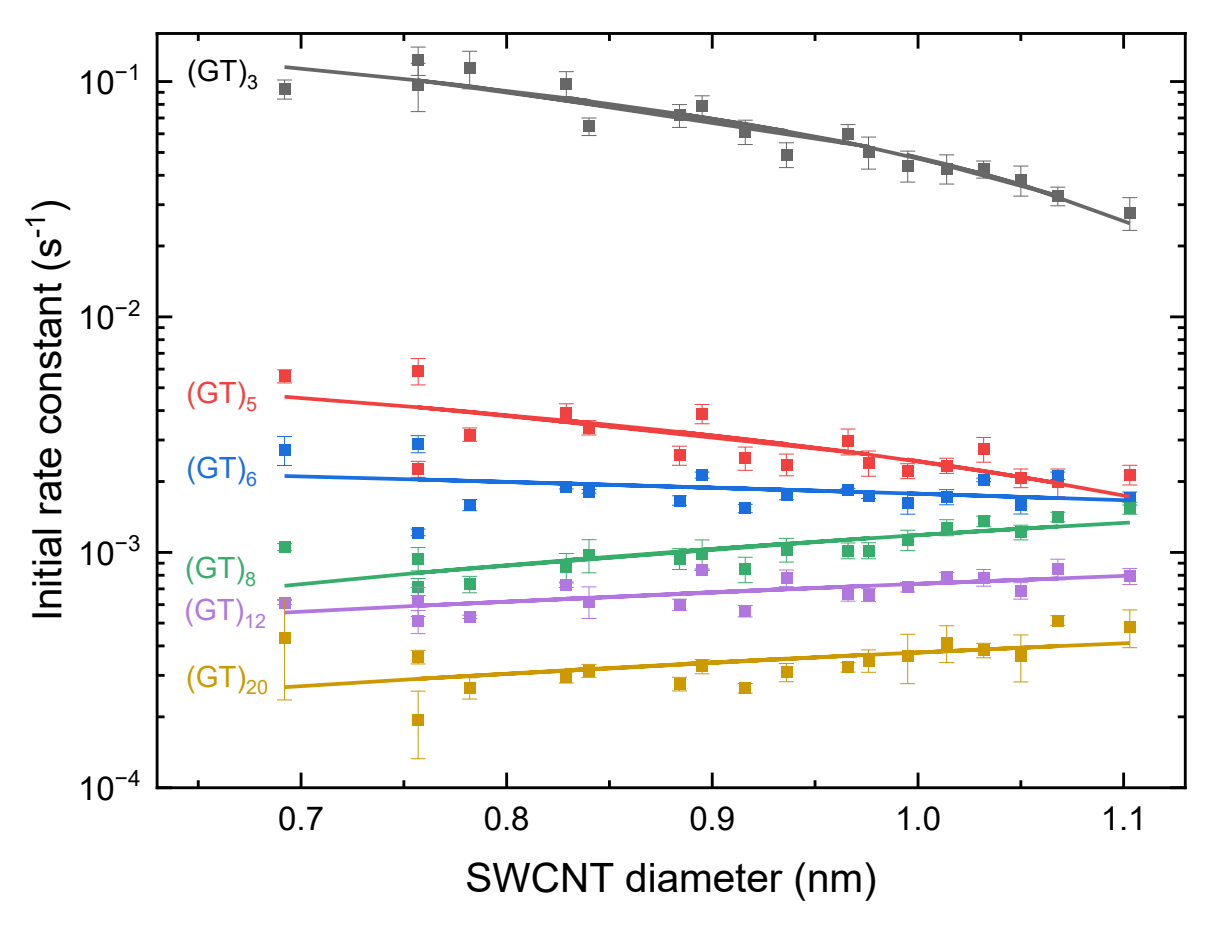


**Figure 4.** Measured initial rate constants as a function of SWCNT diameter for the displacement of SDS by six  $(GT)_n$  oligos, with n equal to 3, 5, 8, 12, and 20, as labeled. Note the logarithmic y-axis scale. Error bars show standard deviations from three replicate experiments.

(which is just 1 by normalization). To find the initial slope, we fit each normalized intensity trace to the following empirical function

$$I_{norm}(t) = \frac{A}{e^{\gamma t} - B} + C \tag{1}$$

The inset in Figure 3b shows data and such fits at early times. The deduced fit parameters were then used in eq 2 to obtain the derivative at time zero in terms of three parameters. This is the initial rate constant.

$$\left(\frac{dI_{norm}}{dt}\right)_{t=0} = -\frac{\gamma A}{(1-B)^2} \tag{2}$$

We performed this analysis for emission wavelengths characteristic of 18 different (n,m) species and repeated the process for the other five  $(GT)_n$  oligo lengths studied here.

Figure 4 plots the full set of these initial rate constant results vs. nanotube diameter, using a logarithmic y-axis. The most obvious pattern is the dramatic decrease in displacement rates with

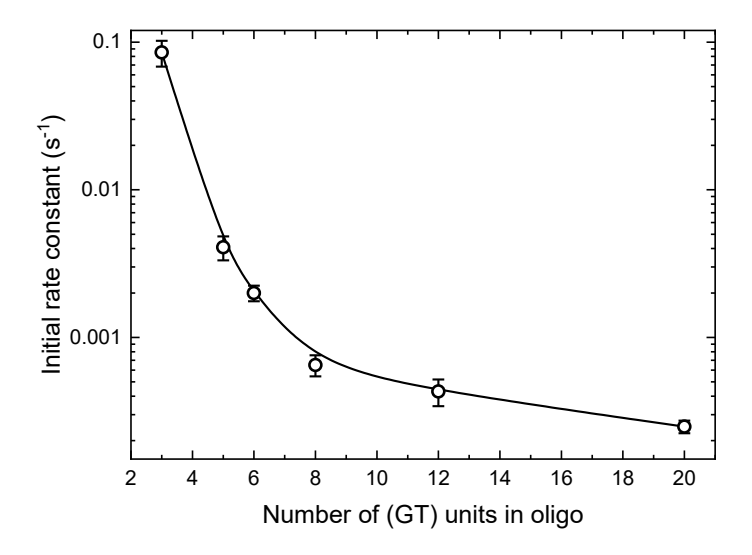


**Figure 5.** Measured initial rate constants for displacement of SDS from (6,5) SWCNTs, plotted vs. the number of (GT) units in the ssDNA oligo. Note the logarithmic y-axis scale. Symbols show data; error bars are standard deviations based on triplicate measurements; and the solid curve is a guide to the eye.

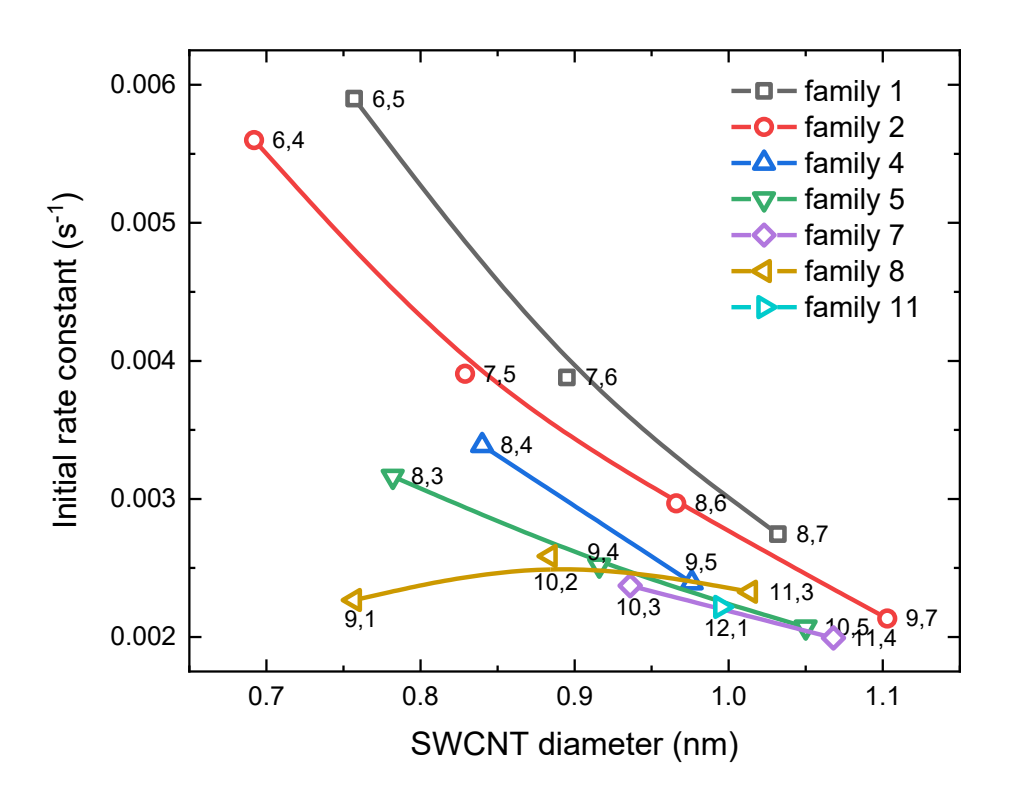


**Figure 6.** Measured initial displacement rate constants for the displacement of SDS from semiconducting SWCNTs by  $(GT)_5$ , plotted versus nanotube diameter. Solid lines connect data points for SWCNTs with the same value of n - m (family index).

increasing ssDNA oligo length. This effect is illustrated for (6,5) nanotubes in Figure 5, which shows that the initial displacement rate drops sharply from (GT)<sub>3</sub> to (GT)<sub>5</sub> and becomes more than a factor of 300 slower for (GT)<sub>20</sub>. Some of this variation can be attributed to the slower diffusional motion of longer ssDNA oligos, which reduces the rates at which they encounter suspended nanotubes. However, we expect this effect to much too weak to explain the large observed range of initial rate constants. For example, results from a prior study suggests that the oligo diffusion coefficients drop from (GT)<sub>3</sub> to (GT)<sub>20</sub> by a factor of only ~3.6.<sup>26</sup>

In addition to the dependence on ssDNA length, Figure 4 also reveals weaker kinetic effects from nanotube structure. In our (GT)<sub>3</sub>, (GT)<sub>5</sub>, and (GT)<sub>6</sub> experiments, larger diameter SWCNTs showed slower displacement. However, this diameter dependence was reversed for the three longer ssDNA oligos studied, (GT)<sub>8</sub>, (GT)<sub>12</sub>, (GT)<sub>20</sub>, for which the larger diameter SWCNTs showed slightly faster initial displacement rate constants.

To qualitatively account for the above findings, we propose a crude two-step kinetic model for the displacement of SDS by ssDNA on nanotube surfaces. The first step is disruption of the adsorbed

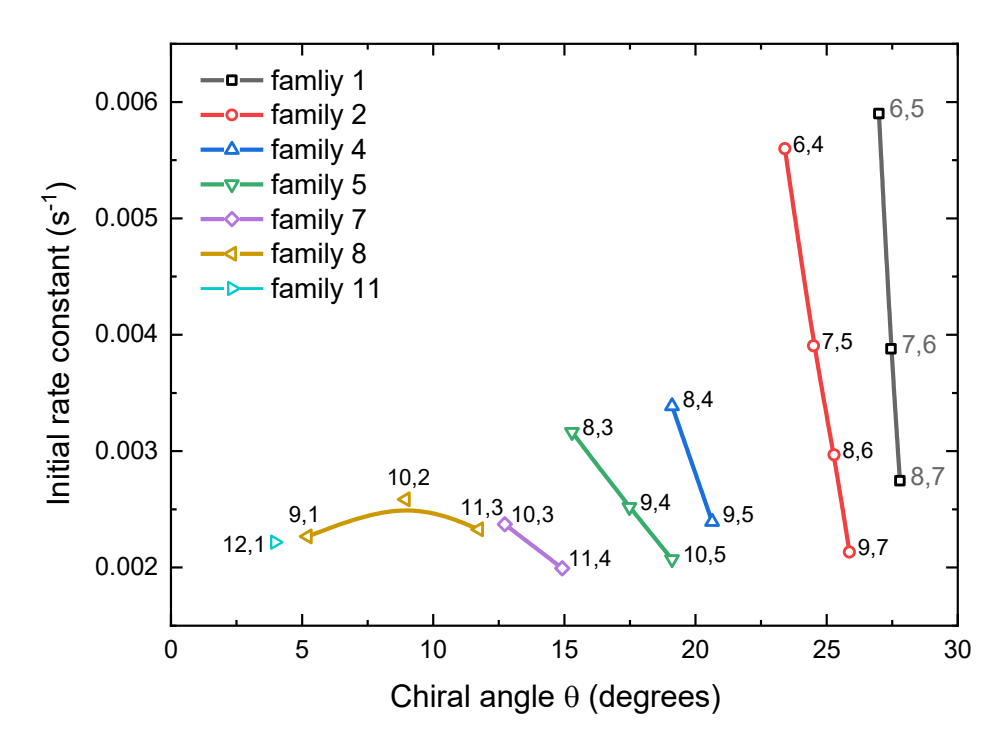


**Figure 7.** Measured initial displacement rate constants for the displacement of SDS from semiconducting SWCNTs by  $(GT)_5$ , plotted versus nanotube chiral angle. Solid lines connect data points for SWCNTs with the same value of n - m (family index).

SDS coating by ssDNA, giving a nanotube coating dominated by ssDNA but still conformationally unrelaxed. We represent this step as

$$SDS / SWCNT + ssDNA \rightarrow SDS + ssDNA* / SWCNT$$
 (step 1)

Here, nanotubes initially coated by SDS are denoted by "SDS / SWCNT" and nanotubes with unrelaxed ssDNA coatings are shown as "ssDNA\* / SWCNT." The second step in our model is relaxation of the nascent ssDNA coatings into more stable conformations that are associated with the final fluorescence spectra.

$$ssDNA* / SWCNT \rightarrow ssDNA / SWCNT$$
 (step 2)

This process may include motions of the guanine and thymine bases to increase pi-pi stacking interactions with the nanotube surface and the emergence of helical or ring-like structures for the ssDNA backbone. We suggest that the rate of this relaxation step decreases for longer ssDNA oligos, which have larger conformational phase spaces. This would make the second step rate-determining for (GT)<sub>8</sub>, (GT)<sub>12</sub>, and (GT)<sub>20</sub> (the longer oligos in our study) whereas the first step is rate-determining for shorter oligos that can more quickly adjust their adsorbed conformations.

A complicating observation, however, is that there is also a kinetic dependence on the nanotube chiral (roll-up) angle,  $\theta$ . This can be seen from Figure 6, where the initial rate constant results are plotted against nanotube diameter. Kinetic points for members of the same n-m family fall on different curves, which lie higher for families with smaller n-m values (chiral angles nearer to armchair structures). In Figure 7 we show this same systematic dependence by plotting directly against chiral angle and drawing curves connecting n-m family members.

For (GT)<sub>5</sub> and (GT)<sub>6</sub>, we find that the combined dependence on nanotube diameter and chiral angle can be rather well expressed by the empirical function

$$k_{initial} = a \left[ \frac{1}{d_t^4 \sqrt{\cos(3\theta)}} \right] + b \tag{3}$$

where  $d_t$  is the nanotube diameter in nanometers,  $\theta$  is the nanotube chiral angle, and a and b are slope and intercept parameters. Figure 8 plots the initial rate constant data for (GT)<sub>5</sub> according to this linearized form. Within the experimental error bars, all points except for (9,1) agree with the fit line obtained by adjusting only the slope and intercept parameters.

If the first step in our kinetic model is rate-limiting for shorter ssDNA oligos, then the systematic variations expressed by eq 3 suggest that SDS displacement is sensitive to nanotube chiral angle. A possible mechanism for this effect is preferential alignment of the SDS alkane tails along the nanotube axis, so that their interactions with the SWCNT  $\pi$ -orbitals will vary with the chiral angle. Such preferential axial alignment has been reported from molecular dynamics simulations of low coverages of SDS adsorbed on SWCNTs, with stronger alignment for smaller diameter SWCNTs.<sup>27</sup> That finding seems consistent with our displacement experiments, which indicate a lower barrier to desorption of SDS molecules at low SDS concentrations on near-armchair, small diameter SWCNTs. Prior studies have deduced that small diameter SWCNTs have a lower affinity for adsorbed SDS than do large diameter SWCNTs.<sup>28,29</sup>

The kinetic variations with chiral angle and diameter expressed by eq 3 are not observed with the oligos (GT)<sub>8</sub>, (GT)<sub>12</sub>, and (GT)<sub>20</sub>, for which the rate determining process is thought to be ssDNA conformational relaxation instead of SDS disruption/displacement. For these oligos, we find a weak opposite dependence on nanotube diameter, with initial rate constants approximately

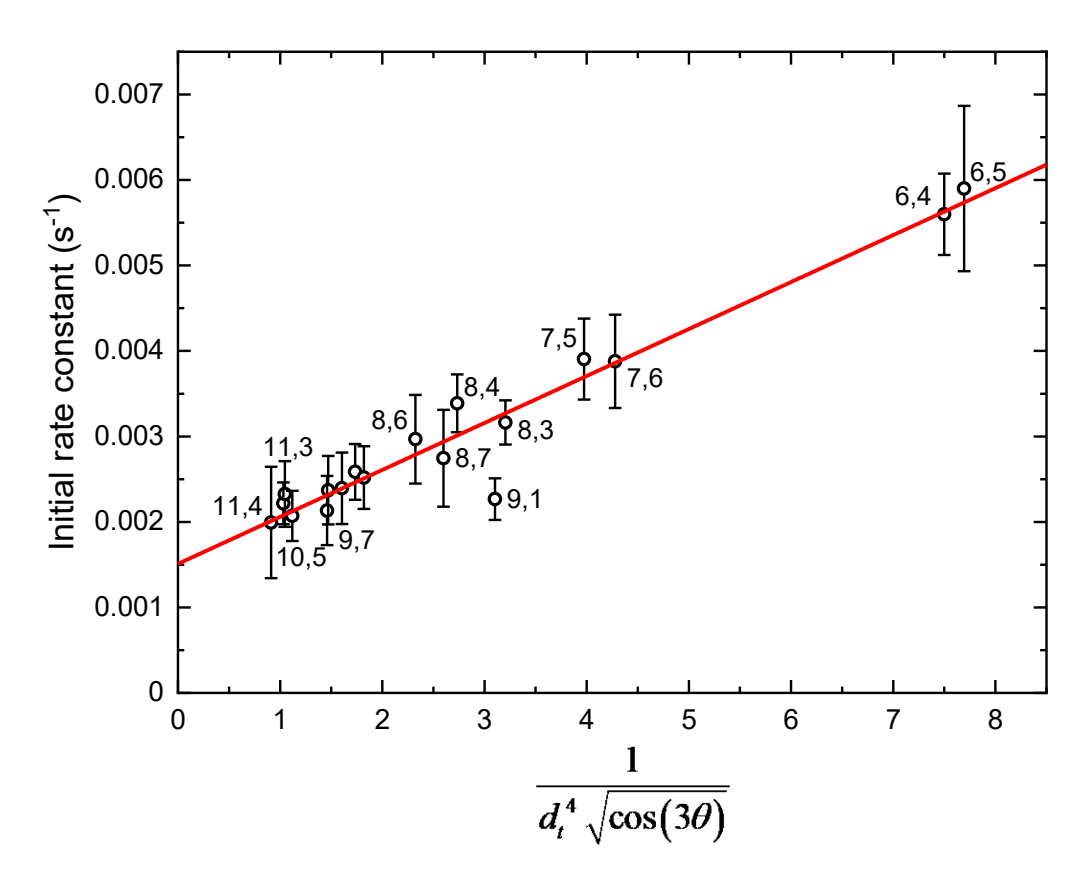


**Figure 8.** Measured initial rate constants for displacement of SDS by  $(GT)_5$  for 18 (n,m) semiconducting SWCNTs. The x-axis values are products of (diameter)<sup>-4</sup> and  $(\cos 3\theta)^{-1/2}$ , where  $\theta$  is the SWCNT chiral angle and SWCNT diameter is in nanometers. Symbols show data points; error bars show standard deviations from triplet runs; and the solid line is a linear best fit, with slope = 0.000549 and intercept = 0.00151.

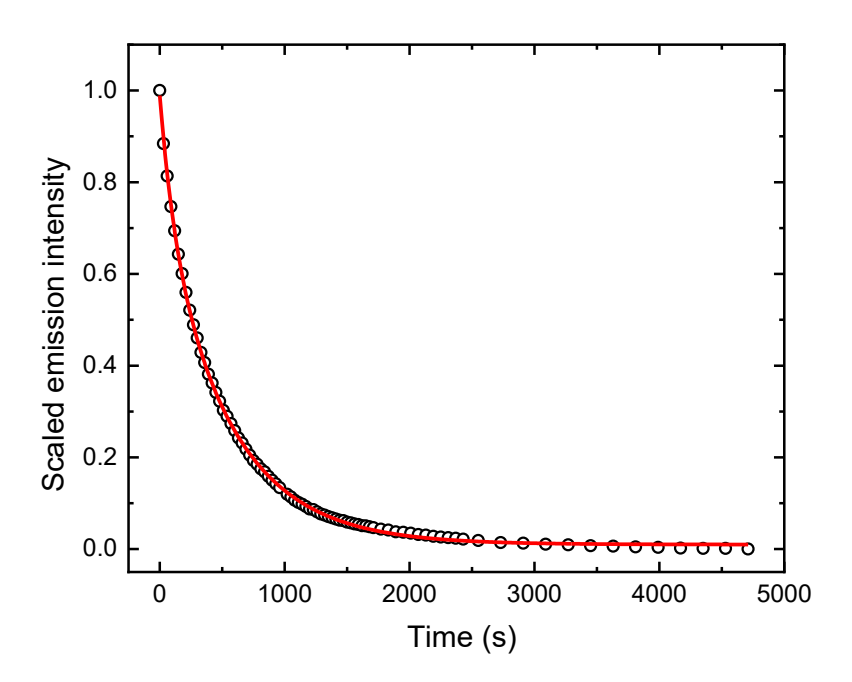
proportional to diameter. Assuming that the helical pitch of the wrapping ssDNA strand remains the same, larger diameter nanotubes would be wrapped by fewer turns of the ssDNA strand than smaller diameter nanotubes, possibly presenting a lower entropic barrier to relaxation.

## **Full Trace Kinetic Analysis**

The full kinetic traces were found to deviate from first order for all combinations of ssDNA oligos and (n,m) species. Nearly all traces could be well represented by a sum of two exponential components:

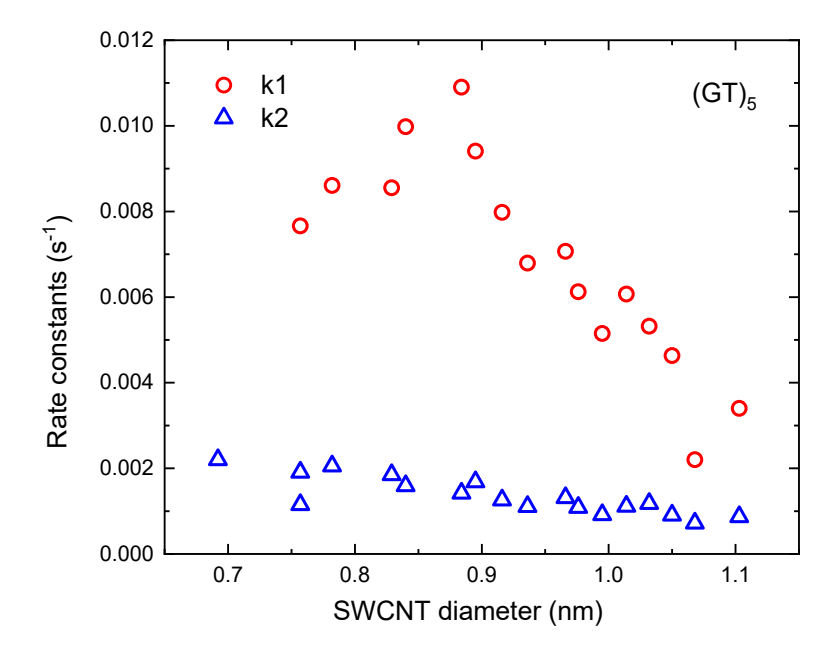
$$y = A_1 e^{-k_1 t} + A_2 e^{-k_2 t}$$

Figure 9 shows such a biexponential fit for the displacement of SDS on (7,5) SWCNTs by  $(GT)_5$ . We have performed similar fits for the range of SWCNT species and oligos studied here and then used the parameters to find times needed for 90% displacement of the SDS. The results, which may help to guide coating displacement protocols, are listed in Table S3 and graphed in Figure S30. For displacement by  $(GT)_5$ , we plot the deduced values of  $k_1$  and  $k_2$  vs. SWCNT diameter in Figure 10, and the ratio  $k_1/k_2$  vs. diameter in Figure 11. (We define  $k_1$  as the larger rate constant.) Both  $k_1$  and  $k_2$  generally tend to smaller values as SWCNT diameter increases, a pattern consistent with the trend in initial rate constants illustrated in Figure 4. We do not assign the two kinetic



**Figure 9.** Full kinetic trace for the displacement of SDS from (7,5) SWCNTs by (GT)<sub>5</sub>. Symbols show normalized fluorescence intensities and the solid curve shows the best-fit biexponential decay function.

components to the different steps in our proposed mechanism. Instead, we suggest that the rate-



**Figure 10.** The dependence of rate constants  $k_1$  and  $k_2$  on SWCNT diameter, based on biexponential best fits of full kinetic traces for displacement of SDS by (GT)<sub>5</sub>. The larger rate constant is labeled  $k_1$ .

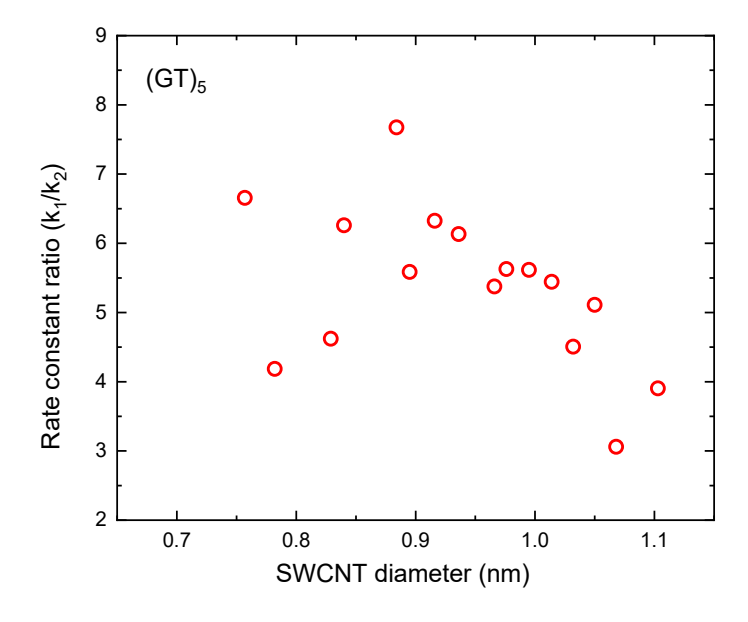


**Figure 11.** Ratios of biexponential rate constants  $k_1 / k_2$  for the displacement of SDS by (GT)<sub>5</sub>, plotted as a function of SWCNT diameter.

determining step (SDS disruption/displacement in the case of (GT)<sub>5</sub>) is not a simple first order process. Inhomogeneities in initial SDS coatings as well as a nonlinear relation between intensity

changes and extent of displacement may lead to a distribution of experimental rate constants that can be modeled by sums of exponential functions.

An alternative interpretation of biexponential decay is that the two enantiomers of each (n,m) species have different displacement kinetics, as has been previously observed for displacement of ssDNA on (7,5) and (6,5) enantiomers.<sup>20,21</sup> Because (n,m) enantiomers can have different surface coverages and fluorescence quantum yields, the biexponential amplitude factors may not be equal even for racemic samples. As shown in Figure 12, the observed  $A_1/A_2$  ratios fall mostly between 0.2 and 0.7. Recalling that we define biexponential component 1 as having the larger decay constant, this interpretation implies that enantiomers with faster displacement rates showed smaller decreases in emissive quantum yield when ssDNA displaced the SDS coating. Those smaller decreases in yield imply more complete surface coverage by the ssDNA coating, which seems consistent with a higher ssDNA adsorption affinity and a lower kinetic barrier to the displacement process. In the limit of large SWCNT diameter, one might expect enantiomeric property differences to decrease, allowing the  $k_1/k_2$  and  $A_1/A_2$  ratios to approach one. The data in Figures 11 and 12 appear consistent with that trend. Future displacement studies on enantiomerically sorted

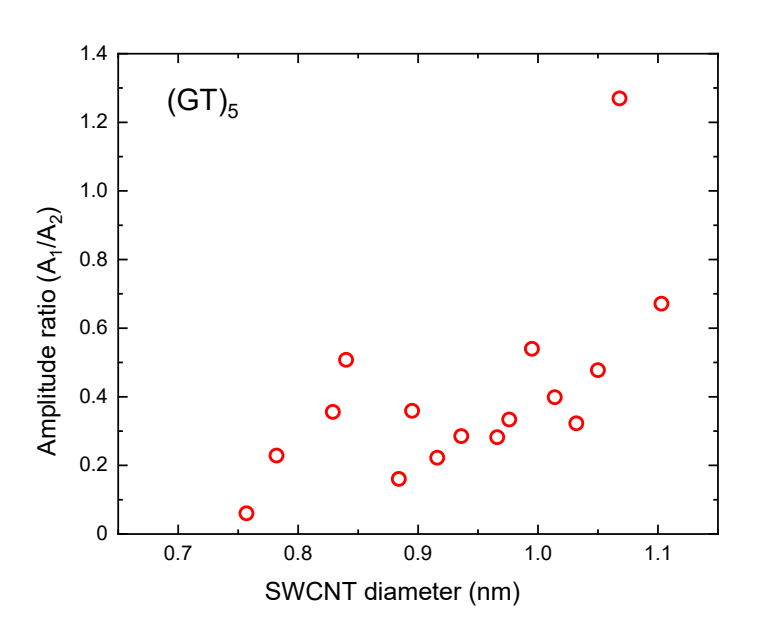


**Figure 12.** Ratios of biexponential amplitudes  $A_1 / A_2$  for the displacement of SDS by (GT)5, plotted as a function of SWCNT diameter.

SWCNT samples should be able to confirm or refute this hypothesis that enantiomeric differences cause the observed biexponential kinetics.

## **CONCLUSIONS**

In this study we have spectroscopically measured the structure-resolved kinetics for displacement of adsorbed SDS by ssDNA (GT)<sub>n</sub> oligos on single-wall carbon nanotube surfaces. The strongest kinetic dependence is on oligo length, with far faster displacements by shorter oligos. The initial rate constants also depend on SWCNT diameter: shorter oligos displace more rapidly on small nanotube diameters, but longer oligos show the opposite dependence. Moreover, the kinetics also depend systematically on SWCNT chiral angle, with faster displacements on near-armchair structures. To qualitatively account for the results, we propose a simplified two-step kinetic model involving disruption of the original SDS coating followed by conformational relaxation of the nascent ssDNA coating. For ssDNA oligos shorter than 12 base pairs, the relaxation is fast enough that the first step is rate-determining. However, for longer oligos, conformational relaxation is much slower and becomes the rate-determining step. Finally, analysis of full kinetic traces shows non-exponential forms that may reflect enantiomeric differences in displacement kinetics for individual (n,m) species. In the future, the complex kinetic dependencies revealed in this study may enable further methods for structure-selective nanotube processing.

## **METHODS / EXPERIMENTAL**

#### **SWCNT** sample preparation

SWCNTs used in this study were taken from batch 195.1 produced by the Rice University HiPco reactor. To prepare pristine SDS-coated samples, raw HiPco SWCNTs were weighed and added to a 0.15% (w/v) aqueous solution of sodium dodecyl sulfate (Acros). The SDS to SWCNT mass ratio at the beginning of sample preparation was kept at approximately 6:1 for all samples. The mixture was immersed in an ice water bath and tip-sonicated at 0.5 W/mL output power (3 mm tip, Misonix Microson XL) for 45 active min (90 min total with a duty cycle of 30 seconds on, 30 seconds off). The SWCNT suspensions were then ultracentrifuged for 4 h at 50000×g in an Optima MAX ultracentrifuge (Beckman Coulter). The top 80 percent of supernatant was collected and stored in sealed vials to give our 0.15% SDS-coated SWCNT stock suspension.

#### DNA sample preparation

Custom-synthesized ssDNA oligonucleotides were purchased from Integrated DNA Technologies, Inc. To prepare ssDNA solutions, 0.1 M sodium chloride solution was added to the tube containing known masses of ssDNA, and the tube was shaken to give complete dissolution. The ratio of DNA mass to NaCl solution was controlled to give a stock concentration of  $10 \mu g/\mu L$ . The DNA stock solution was kept refrigerated, and its concentration was confirmed before each use by UV absorption spectroscopy.

## Trolox solution preparation

Solid Trolox was purchased from Acros Organics. In order to prepare a solution concentration of 5 mmol/L, approximately 1.25 mg of Trolox was weighed and dissolved in 1 mL of ethanol (Decon Laboratories, Inc.). The stock solution was stored in a sealed vial in a refrigerator.

#### Sample characterization

To characterize pristine SDS-suspended HiPco samples, their absorption and near-infrared (NIR) fluorescence spectra were measured in a 10×10 mm cell using a prototype model NS3 NanoSpectralyzer (Applied NanoFluorescence, LLC). Fluorescence spectra were excited by diode lasers emitting at 532, 638, 671, and 779 nm. To measure full excitation-emission maps, we used a different, custom-built instrument. Its tunable excitation source was a spectrally filtered supercontinuum laser (SuperK Extreme, NKT Photonics), and NIR sample emission was detected by a TE cooled InGaAs array spectrometer (BWTek, Sol 1.7). We characterized the ssDNA solutions by UV-vis absorption spectroscopy, using a 10 mm path length cell and a Cary 60 spectrophotometer (Agilent Technologies).

#### **Kinetic spectroscopy**

Time-dependent NIR fluorescence spectra were measured using the custom-built instrument with tunable excitation. We loaded 1 mL of the SDS-SWCNT stock suspension into a  $10\times10$  mm fused silica cuvette, added 1  $\mu$ L of Trolox stock solution to prevent oxidation during measurements, and placed the cuvette into the instrument. The spectral acquisition process was begun and a syringe was used to inject and mix  $200~\mu$ g ( $20~\mu$ L  $\times$   $10~\mu$ g/uL) of ssDNA to start the coating displacement process. The instrument's excitation source was programmed to sequence through as many as five selected wavelengths (580, 640, 674, 727, and 790 nm) during every measurement cycle. At each

of these wavelengths, the sample's emission spectrum was measured by averaging 4 acquisitions

of 200 ms. This measurement cycle was repeated at specified intervals (between 5 s and 1 h) to

compile spectral kinetics for runs ranging from 2 min to 24 h, dependent on the sample. The sample

temperature was approximately 21.6 °C during these runs. The custom-synthesized ssDNA oligos

used for displacement were (GT)<sub>3</sub>, (GT)<sub>5</sub>, (GT)<sub>6</sub>, (GT)<sub>8</sub>, (GT)<sub>12</sub>, and (GT)<sub>20</sub>. Note that we injected

the same mass of ssDNA (200 µg/mL) for all displacement experiments to keep the number of

added (GT) units constant. Triplicate kinetic displacement runs were performed for each of the

oligos.

ASSOCIATED CONTENT

Supporting Information. Table with 108 measured displacement initial rate constants; table and

plot with estimated times for 90% complete displacement; additional plots of fluorescence spectra

and kinetics; graphs of data and structure-dependent fits for displacement by (GT)6; biexponential

fit parameters vs. SWCNT diameter for (GT)6, (GT)8, (GT)12, and (GT)20; plots showing

correlations between initial rate constants for different (GT)<sub>n</sub> oligos.

**AUTHOR INFORMATION** 

**Corresponding Author** 

\*E-mail: weisman@rice.edu. Tel: 713-348-3709

**ORCID** 

Kunhua Lei: 0000-0003-1779-1315

Sergei M. Bachilo: 0000-0001-5236-1383

R. Bruce Weisman: 0000-0001-8546-9980

**Notes** 

The authors declare the following competing financial interest: R.B.W. has a financial interest in

Applied NanoFluorescence, LLC, which manufactures some of the instruments used in this

project.

ACKNOWLEDGMENT

This research was supported by grant CHE-2203309 from the National Science Foundation.

17

#### REFERENCES

- (1) Ouyang, M.; Huang, J.-L.; Lieber, C. M. Fundamental Electronic Properties and Applications of Single-Walled Carbon Nanotubes. *Acc. Chem. Res.* **2002**, *35*, 1018–1025.
- (2) Odom, T. W.; Huang, J. L.; Kim, P.; Lieber, C. M. Atomic Structure and Electronic Properties of Single-Walled Carbon Nanotubes. *Nature* **1998**, *391*, 62–64.
- (3) Kataura, H.; Kumazawa, Y.; Maniwa, Y.; Umezu, I.; Suzuki, S.; Ohtsuka, Y.; Achiba, Y. Optical Properties of Single-Wall Carbon Nanotubes. *Synth. Met.* **1999**, *103*, 2555–2558.
- (4) Salvetat, J.-P.; Bonard, J.-M.; Thomson, N. H.; Kulik, A. J.; Forró, L.; Benoit, W.; Zuppiroli, L. Mechanical Properties of Carbon Nanotubes. *Appl. Phys. A* **1999**, *69*, 255–260.
- (5) Saraireh, S. A.; Tarawneh, M. A.; Chen, R. S.; Alsobhi, B. O.; Shahdan, D.; Gan, S.; Moosavi, S. Chapter 14 Chemical Properties of Carbon Nanotubes. In *Graphene, Nanotubes and Quantum Dots-Based Nanotechnology*; Al-Douri, Y., Ed.; Elsevier: Amsterdam, **2022**; pp 281–304.
- (6) Zheng, M.; Jagota, A.; Semke, E. D.; Diner, B. A.; McLean, R. S.; Lustig, S. R.; Richardson, R. E.; Tassi, N. G. DNA-Assisted Dispersion and Separation of Carbon Nanotubes. *Nat Mater* **2003**, *2*, 338–342.
- (7) Zheng, M.; Jagota, A.; Strano, M. S.; Santos, A. P.; Barone, P.; Chou, S. G.; Diner, B. A.; Dresselhaus, M. S.; McLean, R. S.; Onoa, G. B.; Samsonidze, G. G.; Semke, E. D.; Usrey, M.; Watts, D. J. Structure-Based Carbon Nanotube Sorting by Sequence-Dependent DNA Assembly. *Science* **2003**, *302*, 1545–1548.
- (8) Tu, X.; Manohar, S.; Jagota, A.; Zheng, M. DNA Sequence Motifs for Structure-Specific Recognition and Separation of Carbon Nanotubes. *Nature* **2009**, *460*, 250–253.
- (9) Ao, G.; Khripin, C. Y.; Zheng, M. DNA-Controlled Partition of Carbon Nanotubes in Polymer Aqueous Two-Phase Systems. *J. Am. Chem. Soc.* **2014**, *136*, 10383–10392.
- (10) Lin, C.-W.; Yang, H.; Sanchez, S. R.; Mao, W.; Pang, L.; Beckingham, K. M.; Bast, R. C., Jr.; Weisman, R. B. In Vivo Optical Detection and Spectral Triangulation of Carbon Nanotubes. *ACS Appl. Mater. Interfaces* **2017**, 41680–41690.
- (11) Chen, R. J.; Bangsaruntip, S.; Drouvalakis, K. A.; Wong Shi Kam, N.; Shim, M.; Li, Y.; Kim, W.; Utz, P. J.; Dai, H. Noncovalent Functionalization of Carbon Nanotubes for Highly Specific Electronic Biosensors. *Proc. Natl. Acad. Sci.* **2003**, *100*, 4984–4989.
- (12) So, H. M.; Won, K.; Kim, Y. H.; Kim, B. K.; Ryu, B. H.; Na, P. S.; Kim, H.; Lee, J. O. Single-Walled Carbon Nanotube Biosensors Using Aptamers as Molecular Recognition Elements. *J. Am. Chem. Soc.* **2005**, *127*, 11906–11907.
- (13) Lin, Y.; Lu, F.; Tu, Y.; Ren, Z. Glucose Biosensors Based on Carbon Nanotube Nanoelectrode Ensembles. *Nano Lett.* **2004**, *4*, 191–195.
- (14) Dwyer, C.; Guthold, M.; Falvo, M.; Washburn, S.; Superfine, R.; Erie, D. DNA-Functionalized Single-Walled Carbon Nanotubes. *Nanotechnology* **2002**, *13*, 601.
- (15) Zheng, Y.; Bachilo, S. M.; Weisman, R. B. Controlled Patterning of Carbon Nanotube Energy Levels by Covalent DNA Functionalization. *ACS Nano* **2019**, *13*, 8222–8228.

- (16) Jovanović, S. P.; Marković, Z. M.; Kleut, D. N.; Romčević, N. Z.; Trajković, V. S.; Dramićanin, M. D.; Todorović Marković, B. M. A Novel Method for the Functionalization of γ-Irradiated Single Wall Carbon Nanotubes with DNA. *Nanotechnology* 2009, 20, 445602.
- (17) Roxbury, D.; Tu, X.; Zheng, M.; Jagota, A. Recognition Ability of DNA for Carbon Nanotubes Correlates with Their Binding Affinity. *Langmuir* **2011**, *27*, 8282–8293.
- (18) Shankar, A.; Mittal, J.; Jagota, A. Binding between DNA and Carbon Nanotubes Strongly Depends upon Sequence and Chirality. *Langmuir* **2014**, *30*, 3176–3183.
- (19) Jena, P. V.; Safaee, M. M.; Heller, D. A.; Roxbury, D. DNA-Carbon Nanotube Complexation Affinity and Photoluminescence Modulation Are Independent. ACS Appl. Mater. Interfaces 2017, 9, 21397–21405.
- (20) Zheng, Y.; Bachilo, S. M.; Weisman, R. B. Enantiomers of Single-Wall Carbon Nanotubes Show Distinct Coating Displacement Kinetics. *J. Phys. Chem. Lett.* **2018**, *9*, 3793–3797.
- (21) Xhyliu, F.; Ao, G. Chirality-Pure Carbon Nanotubes Show Distinct Complexation with Recognition DNA Sequences. *Carbon* **2020**, *167*, 601–608.
- (22) Yang, Y.; Sharma, A.; Noetinger, G.; Zheng, M.; Jagota, A. Pathway-Dependent Structures of DNA-Wrapped Carbon Nanotubes: Direct Sonication vs Surfactant/DNA Exchange. J. Phys. Chem. C 2020, 124, 9045–9055.
- (23) O'Connell, M. J.; Bachilo, S. M.; Huffman, C. B.; Moore, V. C.; Strano, M. S.; Haroz, E. H.; Rialon, K. L.; Boul, P. J.; Noon, W. H.; Kittrell, C.; Ma, J. P.; Hauge, R. H.; Weisman, R. B.; Smalley, R. E. Band Gap Fluorescence from Individual Single-Walled Carbon Nanotubes. *Science* **2002**, *297*, 593–596.
- (24) Bachilo, S. M.; Strano, M. S.; Kittrell, C.; Hauge, R. H.; Smalley, R. E.; Weisman, R. B. Structure-Assigned Optical Spectra of Single-Walled Carbon Nanotubes. *Science* **2002**, *298* (5602), 2361–2366. https://doi.org/10.1126/science.1078727.
- (25) Weisman, R. B.; Bachilo, S. M. Dependence of Optical Transition Energies on Structure for Single-Walled Carbon Nanotubes in Aqueous Suspension: An Empirical Kataura Plot. *Nano Lett.* **2003**, *3*, 1235–1238.
- (26) Nkodo, A. E.; Garnier, J. M.; Tinland, B.; Ren, H.; Desruisseaux, C.; McCormick, L. C.; Drouin, G.; Slater, G. W. Diffusion Coefficient of DNA Molecules during Free Solution Electrophoresis. *Electrophoresis* **2001**, *22*, 2424–2432.
- (27) Tummala, N. R.; Striolo, A. SDS Surfactants on Carbon Nanotubes: Aggregate Morphology. *ACS Nano* **2009**, *3*, 595–602.
- (28) Liu, H.; Nishide, D.; Tanaka, T.; Kataura, H. Large-Scale Single-Chirality Separation of Single-Wall Carbon Nanotubes by Simple Gel Chromatography. *Nat. Commun.* **2011**, *2*, 309.
- (29) Subbaiyan, N. K.; Cambre, S.; Parra-Vasquez, A. N. G.; Haroz, E. H.; Doorn, S. K.; Duque, J. G. Role of Surfactants and Salt in Aqueous Two-Phase Separation of Carbon Nanotubes toward Simple Chirality Isolation. *ACS Nano* **2014**, *8*, 1619–1628.

# Table of Contents Graphic

